Supplementary Materials for

In vivo Non-Invasive Confocal Fluorescence Imaging Beyond 1700 nm Using Superconducting Nanowire Single-Photon Detectors

Feifei Wang, Fuqiang Ren, Zhuoran Ma, Liangqiong Qu, Ronan Gourgues, Chun Xu, Ani Baghdasaryan, Jiachen Li, Iman Esmaeil Zadeh, Johannes WN Los, Andreas Fognini, Jessie Qin-Dregely and Hongjie Dai

Correspondence to: hdai@stanford.edu

SUPPLEMENTARY VIDEO CAPTIONS

Supplementary Video 1 | Animated mouse brain video from non-invasive in vivo NIR-IIc confocal microscopy images of vasculatures in intact mouse head. The volumetric imaging was done using a 1540 nm-illumination for one-photon excitation and 1750-2000 nm detection for NIR-IIc P^3-QDc circulating in brain vasculatures. The video here shows 3D images of intact mouse head with clearly resolved scalp, skull, meninges and brain cortex layers taken with 5-μm *z* increment in depth. The imaging time for each z-plane was linearly increased from 5 s to 30 s. A 25X objective (NA = 1.05) was used.

SUPPLEMENTARY NOTE 1

SNSPD for NIR-IIc imaging

In the SNSPD system, detectors with cavities based on an Au back mirror with a SiO_2 $\lambda/4$ (λ is the wavelength) spacer between the mirror and the superconducting film, and cavities based on a Distributed Bragg Reflector (DBR) were constructed[1]. These two types of detectors with different cavities performed similarly in terms of efficiency and dark-counts in the wavelength range of 1550-2000 nm (Fig, 1f,g). The specially designed SNSPD showed a system detection efficiency (SDE) of ~ 50% to 75% in the NIR-IIb 1500-1700 nm window (Channel 1 and 2) and ~ 25% to 50% in the NIR-IIc 1700-2000 nm window (Channel 3 and 4), respectively (Fig. 1f). These SNSPD were cooled at ~ 3 K Gifford-McMahon Cryocooler. The SNSPD were connected to our home-built confocal microscope through single mode (SM) fibers (~ 10 μm mode field diameter) transmitting in 1200-2000 nm (see Methods and Supplementary Figs. 3 and 4) that also functioned as a pinhole to reject the out-of-focus fluorescence signal. The home-built confocal microscope allowed diffraction-limited resolution in non-scattering media calibrated by observing nanoparticles on a cover glass (see resolution analysis in Methods). The selected SM fiber afforded a natural cut-off for the black-body radiation that significantly reduced the dark-count rate to be ~ 500 Hz and enabled high SBR for NIR-IIc fluorescence imaging (Fig. 1g and Methods). For example, with a similar system equipped with PM2000 fibers (operating wavelength: 1700-2300 nm, Thorlabs) we measured ~10,000 dark-counts per second.

The low timing jitter (< 55 ps) facilitated high temporal single-photon resolution. Note that a previous work employed SNSPD with SDE > 50% at 1064 nm for cerebral vasculature (labeled by the IR820 dyes) imaging through skull with scalp removed in the ~ 1000-1200 nm detection range[2].

Four individual SNSPD chips were mounted in cryostat for NIR-IIb and IIc imaging. These four SNSPD chips were connected to an electronic driver. One SNSPD chip corresponded to one channel (Fig. 1f.g). The SDE and dark count rates of these four SNSPD chips were compared in Fig. 1f.g. The SNSPD chips were mounted in a compact closed-cycle cryostat cooled by a Gifford-McMahon Cryocooler. The temperature of cryostat was stabled as ~ 3 K. The system detection efficiency of the SNSPD was calculated by:

$$SDE = (Counts/IntTime - DarkCounts/IntTime)/(Power \times Attenuation \times Wavelength/(h \times c))$$

where IntTime is integration time, h is Planck constant, c is speed of light in free space and Attenuation is the attenuation on laser adjusted by a digital attenuator.

SUPPLEMENTARY NOTE 2

Laser power analysis

From the American National Standard for Safe Use of Lasers (ANSI Z136.1), the safety limit for 808 nm, 1319 nm, 1540 nm and 1650 nm lasers are 1.8 $t^{0.25}$ J cm^{-2}, 5.5 $t^{0.25}$ J cm^{-2}, 1.0 J cm^{-2} and 1.0 J cm^{-2}, which corresponds to total energy in the spot over illumination dwell time t of 1.8 $A\,t^{-0.75}$ W, 5.5 $A\,t^{-0.75}$ W, $A\,t^{-1}$ W and $A\,t^{-1}$ W, respectively with spot area $A = \pi r^2$, where r is the radius of the focus that can be derived from the point spread function (PSF)[3]. We estimated the PSF in tissue by measuring the FWHM of blood vessels in mouse brain ex vivo (Supplementary Fig. 14). FWHM in lateral direction was ~ 2.0 ± 0.45 μm. The area of focus spot A = ~ 4π μm^2. The radius of laser pattern on sample surface can be calculated by $R = r + z \cdot \tan\alpha$, where $\alpha = \arcsin(\mathrm{NA}/n)$ with the heavy water refractive index n = 1.33 (Supplementary Fig. 15a). Consider the attenuation of laser transmitting in mouse brain (Supplementary Fig. 6c), we can assess the threshold power at brain surface for confocal imaging at each depth (Supplementary Fig. 15b).

We first examined confocal imaging performance at different excitation powers (excitation: 1650 nm, power: 0.76 – 28.5 mW, dwell: 50 μs, Supplementary Fig. 16) or dwell time (excitation: 1650 nm, 0.76 mW, dwell: 12.5 – 750 μs, Supplementary Fig. 17) by NIR-IIc imaging blood vessels in mouse brain ex vivo. Excitation power was measured by a laser power meter (3A-SH, NOVA II, OPHIR).

We employed a method of linearly increasing the laser power at larger imaging depth z to stay below the laser safety limit while maximizing emission signal. An example is ex vivo imaging in the Supplementary Fig. 18, for which the laser power of 1650 nm laser were linearly increased from 1.6 mW to 15.5 mW from z = 0 μm to z = 1500 μm, accompanied by dwell time increase from 19 μs to 57 μs. When imaging depth z = 0 μm, the fluence at brain surface was 0.24 J/cm^2, which was ~ 4 times than the fluence limit (1 J/cm^2). When imaging at z = 1500 μm with 15.5 mW laser power, the beam at the surface expanded to give a fluence of 7.5 x 10^{-6} J/cm^2, which was very small. At z = 1500 mm, the laser power of 15.5 mW decayed to 1.68 mW due to absorption and scattering (see Supplementary Fig. 6 Monte Carlo simulation), giving a fluence of 0.77 J/cm^2, also below the fluence limit (1 J/cm^2). This approach ensures laser safety while maximizing imaging signal at various z inside the tissue.

The same method was applied for imaging iLN in vivo (Fig. 4g, h). In this case, the dwell time and the power of 1650 nm laser were linearly increased from 19 μs to 46 μs and from 1.6 mW to

10.0 mW respectively for larger *z*. Calculations showed that the laser fluence was smaller than the limit of 1 J/cm^2 at all *z*.

SUPPLEMENTARY NOTE 3

Point spread function simulations of confocal microscope

The point spread function (PSF) of confocal microscope ($PSF_{confocal}$) is given by

$$\mathrm{PSF}_{\mathrm{confocal}}\left(\rho,z\right)=\mathrm{PSF}_{\mathrm{i}}\left(\rho,z\right)\times\left(\mathrm{PSF}_{\mathrm{d}}\left(\rho,z\right)*\mathrm{A}_{\mathrm{p}}\right)$$

where PSF_i is the illumination PSF, PSF_d is the detection PSF, and A_p is the pinhole function. The * symbol represents convolution. ρ is the radius in (x,y) plane and z is the z-component of cartesian coordinates.

The illumination point spread function can be modeled by a Gaussian-Lorentzian profile[4]:

$$\mathrm{PSF}_{\mathrm{i}}\left(\rho,z\right)=e^{-2\rho^2/\mathrm{w}_0^2\left(1+\varsigma^2\right)}\Big/\mathrm{z}_R^2\left(1+\varsigma^2\right)$$

where $z_R = \pi w_0^2 \kappa_i$, $\varsigma = z/\pi w_0^2 \kappa_i$, $\kappa_i = n/\lambda_i$, w_0 is the waist of gaussian beam. κ_i is the wavenumber. λ_i is the excitation wavelength. n is the index of refraction of the surrounding medium.

PSF_d can be modeled by circular pupil as[4]:

$$\mathrm{PSF}_{\mathrm{d}}\left(\rho,z\right)=\left|2\pi\int_0^{NA/\lambda_d}\kappa_\perp J_0\left(2\pi\kappa_\perp\rho\right)e^{i2\pi\kappa_d z}e^{-i\pi\frac{z}{\kappa_d}\kappa_\perp^2}d\kappa_\perp\Big/\kappa_{\mathrm{d}}\right|^2$$

where NA is the numerical aperture of objective. λ_d is the emission wavelength. $\kappa_d = n/\lambda_d$. J_0 is the zeroth order cylindrical Bessel function.

The pinhole of confocal microscope can be defined by the unitless aperture function A_p. For a circular aperture of radius a_p, the Fourier transform of the pinhole function can be given as $\mathcal{A}(\vec{\kappa}_\perp)$ = A_p jinc($2\pi\kappa_\perp a_p$), where $A_p = \pi a_p^2$. jinc($2\pi\kappa_\perp\rho$) = $J_1(2\pi\kappa_\perp\rho)/(\pi\kappa_\perp\rho)$, where J_1 is the cylindrical Bessel function of order 1.

SUPPLEMENTARY FIGURES

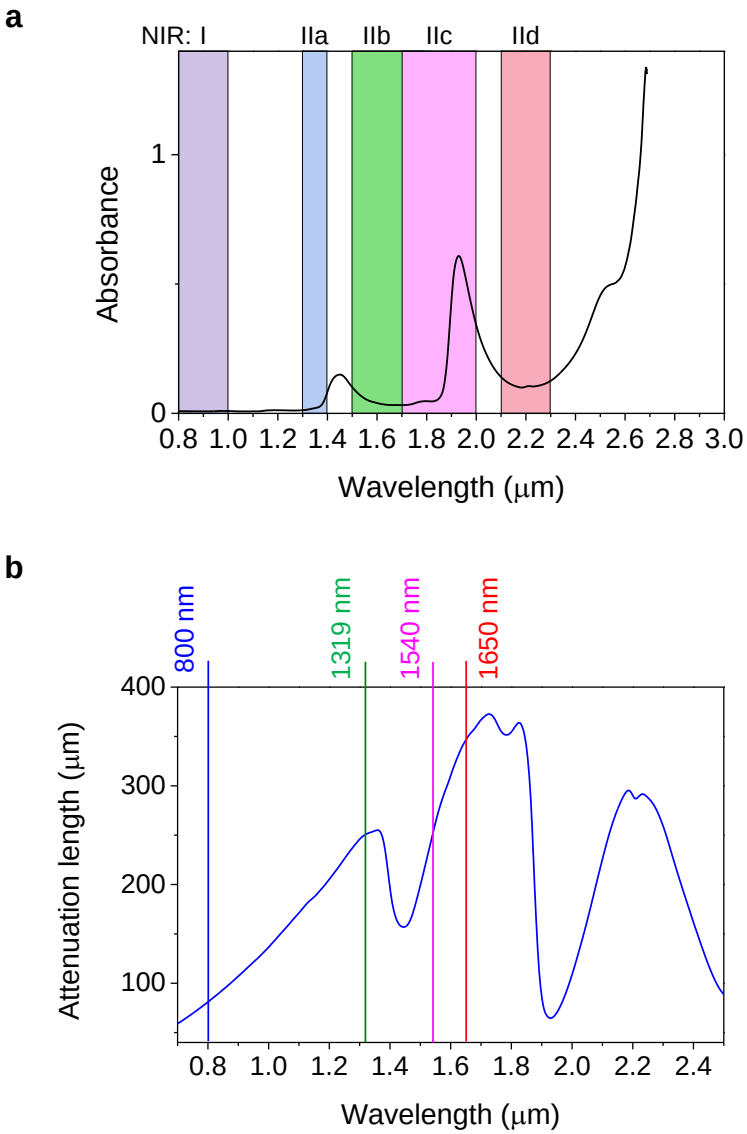

Supplementary Figure 1. (**a**) The absorbance of water measured in a cuvette with 0.1 mm light path. The UV-Vis-NIR absorbance spectrum of water was measured using V-770 Spectrophotometer (JASCO). (**b**) The attenuation lengths at different excitation wavelengths

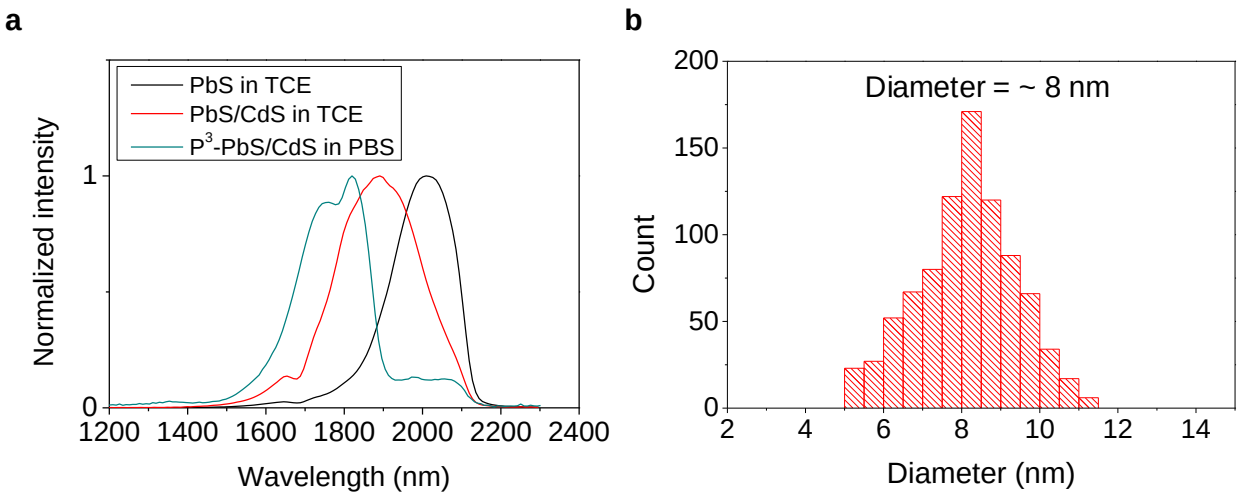

Supplementary Figure 2. Characterization of NIR-IIc core/shell PbS/CdS quantum dots (named 'QDc' in this work). (**a**) Fluorescence emission spectra of PbS core, core/shell PbS/CdS QD in tetrachloroethylene (TCE) and hydrophilic cross-linked P^3 coated PbS/CdS QD in PBS after aqueous transfer. (**b**) Size-distribution histogram of QDc prior to P^3-coating measured from TEM images.

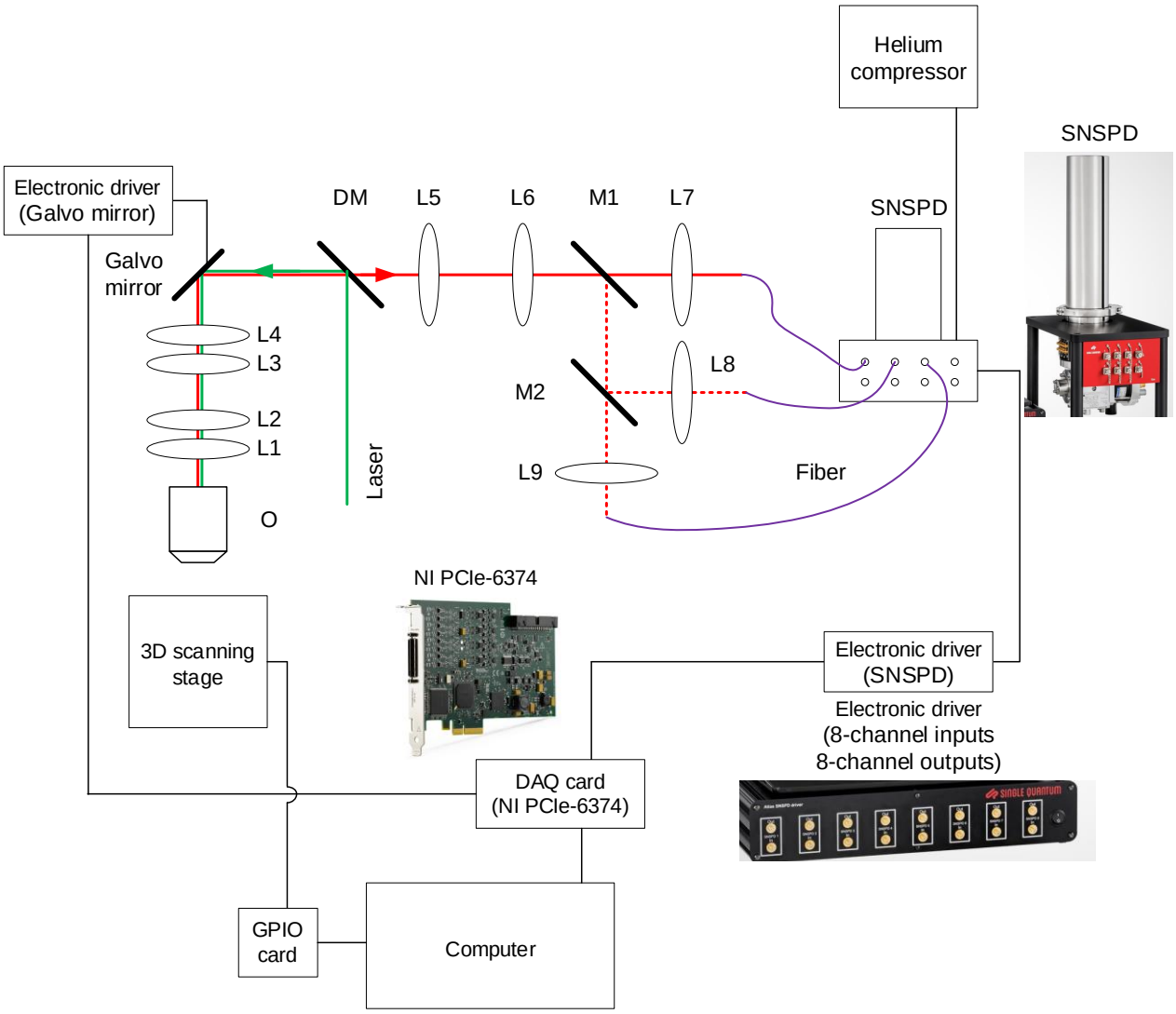

Supplementary Figure 3. A schematic of the confocal microscopy in the second near-infrared window. The components are as follows: objective (O), achromatic lenses (L1 – L9), mirrors (M1, M2), dichroic mirror (DM). Three SNSPD detectors were selected by removable mirrors (M1, M2) A laser beam with wavelength of 808 nm, 1319 nm, 1540 nm or 1650 nm was reflected by a galvo mirror (GVS002, Thorlabs) into a Plössl scan lens (constructed from two achromatic doublets, L3, L4, AC508-150-C, Thorlabs), a Plössl tube lens (constructed from two achromatic doublets, L1, L2, AC508-300-C, Thorlabs) and then focused by an objective into a sample (Supplementary Fig. 2). Fluorescence signal was collected by the same objective, tube lens and scan lens. After de-scanned by the galvo mirror and resized by two achromatic doublets (L5, AC254-100-C and L6, AC508-150-C), the fluorescence light was focused into three single mode (SM) fibers (P1-SMF28E-FC-5, Thorlabs) by achromatic doublets (L7-L9, AC254-030-C, Thorlabs) after filtered by selected emission filters. Then the SM fiber transmitted the fluorescence to NIR-IIb or NIR-IIc SNSPD. Four individual SNSPD chips were mounted in cryostat for NIR-IIb and IIc imaging. These four SNSPD chips were connected to four channels of an 8-channel electronic driver. One SNSPD chip corresponded to one channel (Fig. 1f.g). The SDE and dark count rates of these four SNSPD chips were compared in Fig. 1f.g. The SNSPD chips were mounted in a compact closed-cycle cryostat cooled by a Gifford-McMahon Cryocooler. The galvo mirror, SNSPD and a motorized translation stage (M-VP-25XL, Newport) were synchronized by an acquisition card (NI

PCIe-6374) through Labview. This acquisition card also worked as a photon counter to count the TTL signal generated by SNSPD when photons were detected.

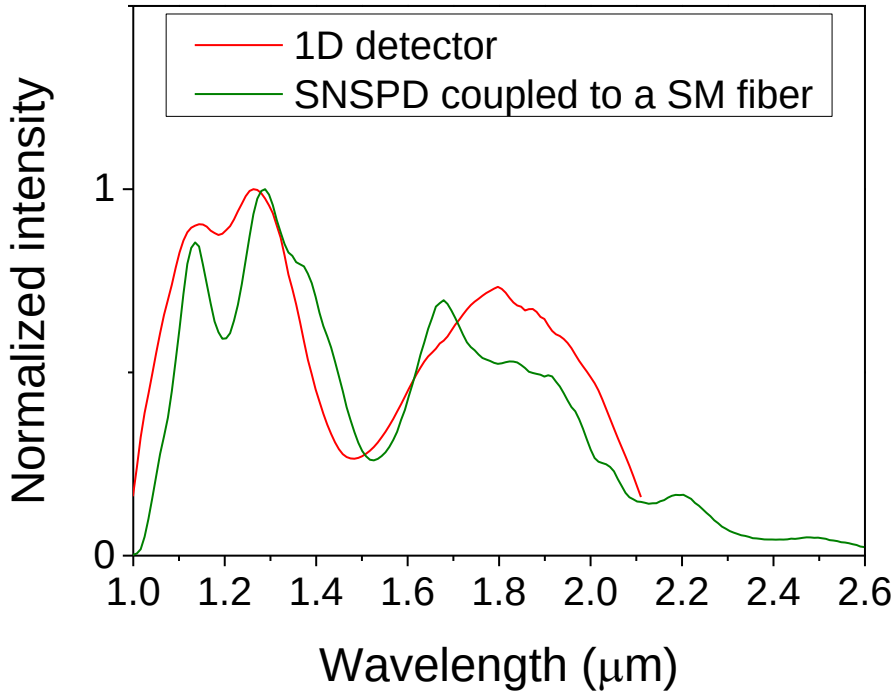

Supplementary Figure 4. Single-mode (SM) fiber used for NIR-IIc confocal microscopy using the SNSPD. We mixed three PbS/CdS QDs of different average sizes to a suspension with emission covering the ~ 1000-2100 nm range. The overall emission spectrum was first measured by a commercial spectrometer with a 1D extended InGaAs camera (Princeton Instruments) without SM fiber coupling as shown by the red curve. The fluorescence was collected by a couple of lenses into the spectrometer. Then the spectrum of the mixed PbS/CdS QDs was measured again using the same spectrometer but connected to SNSPD coupled to a SM fiber (green curve). An 808 nm laser was used to excite the mixed QDs. The fiber used here was P1-SMF28E-FC-5 from Thorlabs with a specification of transmission in the 1260-1625 nm range. Our data here showed that the fiber also allowed transmission in the 1700-2000 nm (NIR-IIc), which was not described in the product datasheet. We tried various fibers and this fiber turned out to be optimal for NIR-IIc confocal imaging using SNSPD. The spectrometer has two outlets allowing to connect to two detectors. One outlet was connected to traditional 1D InGaAs camera. The other outlet was coupled to SNSPD by using a 10-μm core single mode fiber (P1-SMF28E-FC-5). These two outlets can be selected by a motorized mirror inside the spectrometer. A home-made Labview software was used to control the motorized mirror and the grid position in spectrometer to adjust the wavelength that can be achieved from the second outlet. At each grid position corresponding to a wavelength, the SNSPD was controlled to sample an intensity value collected by an acquisition card (NI USB-6210). By changing the grid position continuously, the wavelength can be scanned from 1000 nm to 2600 nm. As we collected all fluorescence intensity values at each wavelength, we can measure the spectrum using SNSPD.

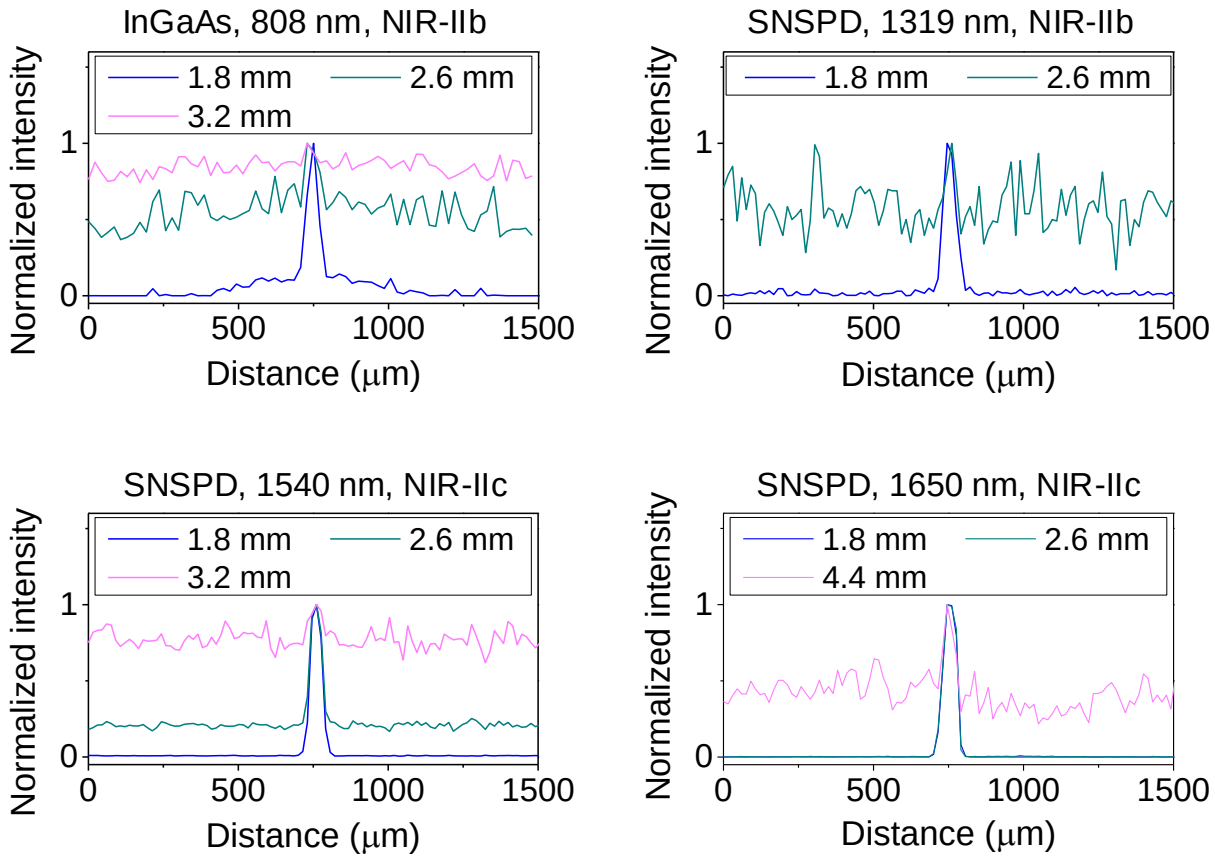

Supplementary Figure 5. Normalized photon counts profiles of the capillary immersed at different depth in the 5% intralipid imaged by a wide-field system or a confocal microscope in NIR-IIb or NIR-IIc window shown in Fig, 2a.

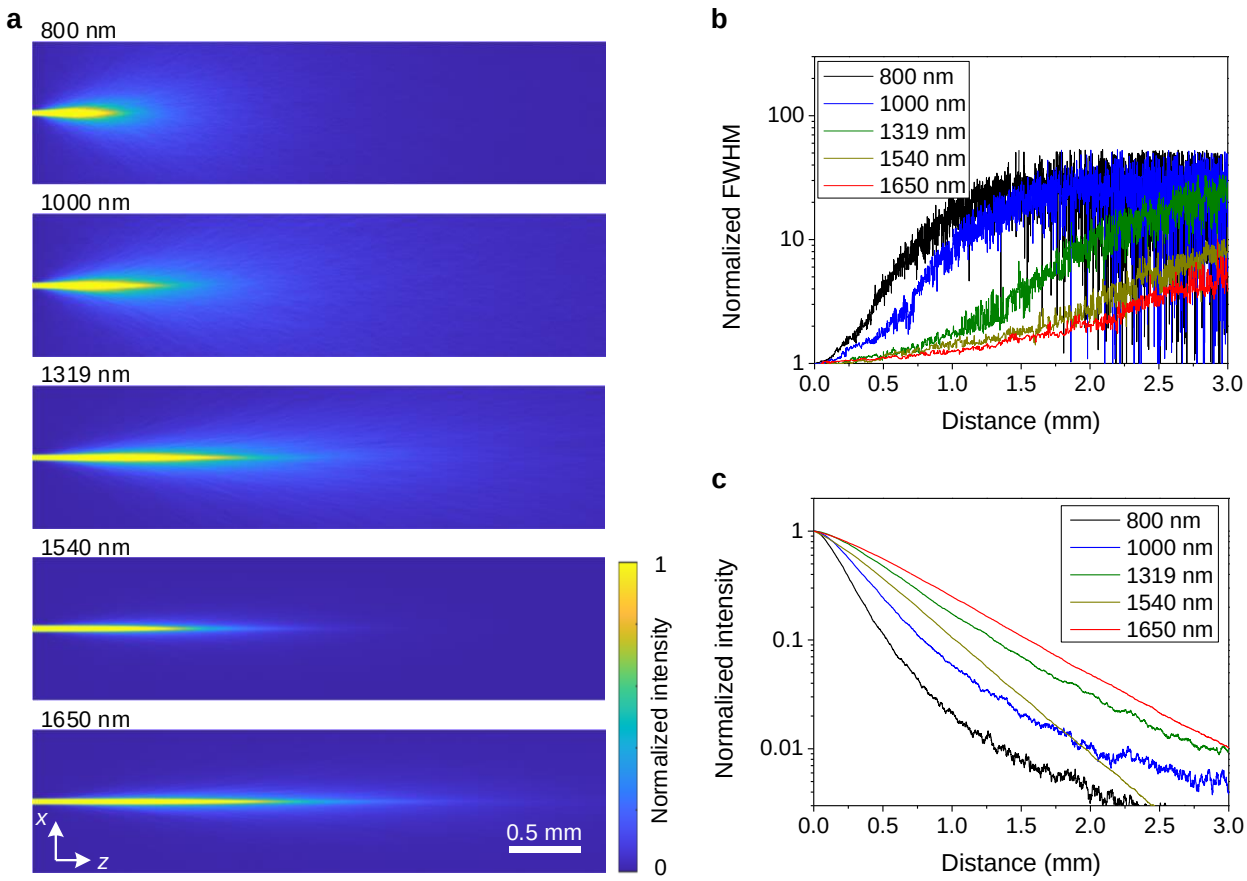

Supplementary Figure 6. (**a**) Monte Carlo simulations [5] of laser beams with different wavelength transmitting in mouse brain. (**b**) FWHM of laser beams along *z* direction. FWHM was normalized by the initial FWHM of laser beams at $z = 0$ mm. Longer wavelength suffered less broadening in FWHM. (**c**) Normalized intensity at the middle of laser beam decayed along *z* direction. 1650 nm laser experienced least broadening and intensity decay as transmitting in mouse brain.

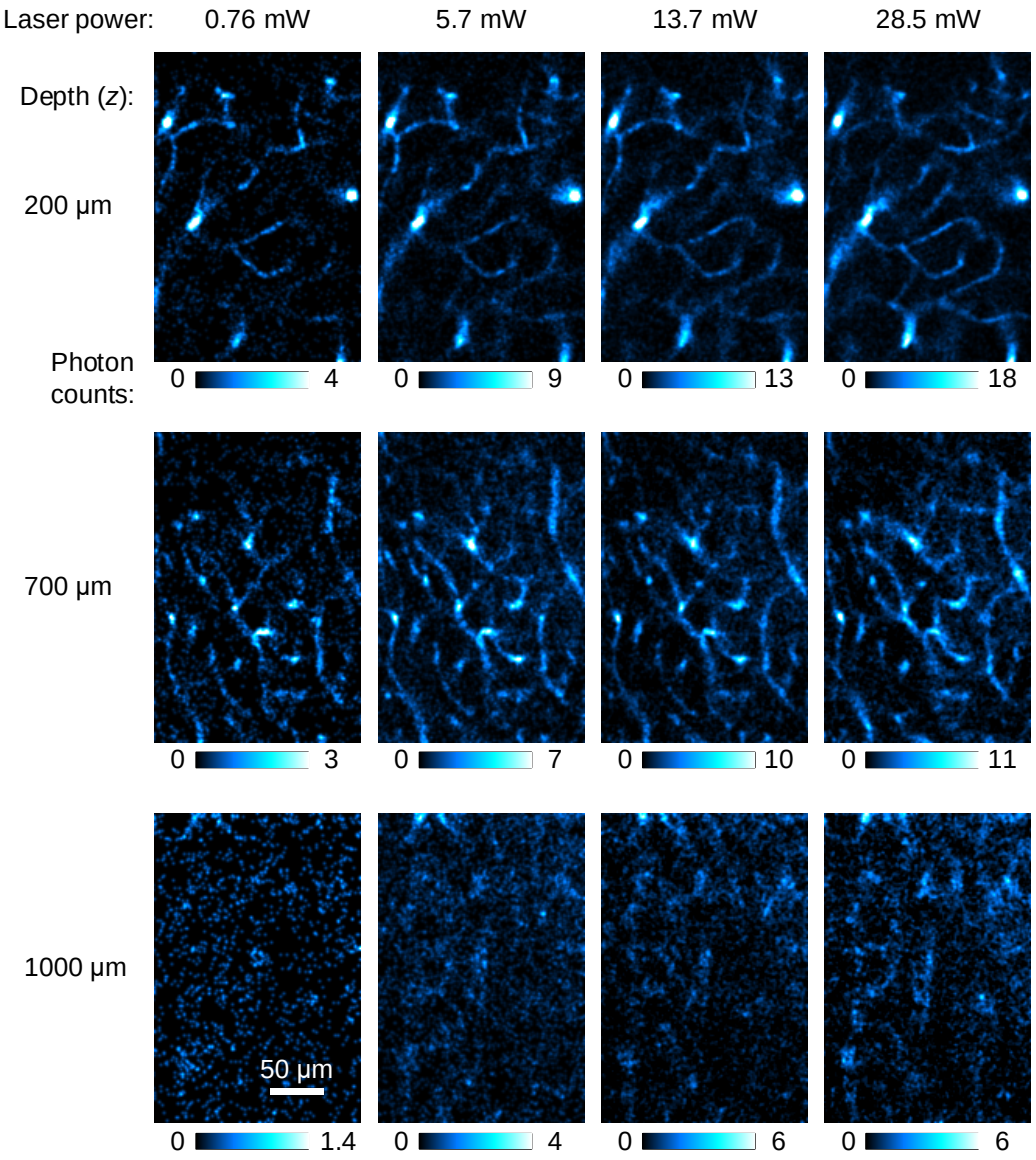

Supplementary Figure 7. Ex vivo NIR-IIc confocal microscopy of blood vessels in mouse brain excited by a 1650 nm laser with different power at 3 Hz (333 ms per frame). The mouse brain tissue sample (n = 2) for ex vivo confocal microscopy was prepared by intravenous injection of free P^3-QDc. The mouse was euthanized under anesthesia 20 min post injection of P^3-QDc while still in circulation. The mouse brain was fixed with 10% neutral-buffered formalin at room temperature and preserved in glycerol at 4 ^oC for ex vivo imaging. A scan rate of ~ 3 Hz (pixels: 133 x 200, scan area: 185 µm x 278 µm) was applied, which was limited by the galvo mirror we used. For 1.0 mm depth volumetric imaging with 5 µm scan step in *z*, the total scan time was ~ 1.1 min.

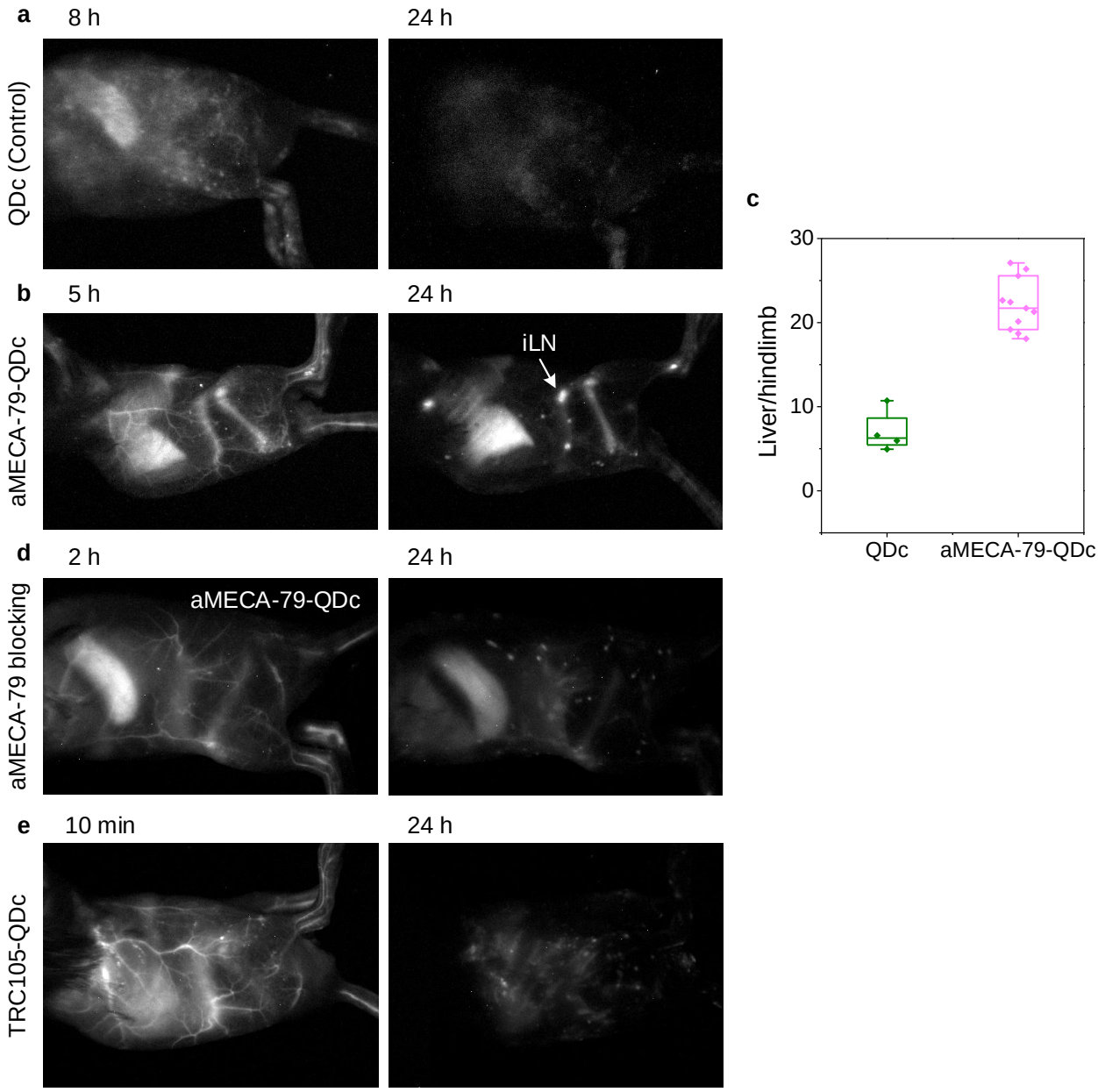

Supplementary Figure 8. Wide-field images of Balb/c mice recorded after intravenous injection of (**a**) free P^3-QDc (mice number = 4) and (**b**) aMECA-79-QDc (mice number = 11) at two different timepoints. (**c**) The ratio of fluorescence signal in liver and hindlimb (reference) measured from mice injected with (**a**) QDc or (**b**) aMECA-79-QDc 24 post injection. Data are presented as box plots (center line, median; interquartile range, 25th and 75th percentile; whiskers, 1.5 × s.d.; points, outliers). (**d**) Wide-field imaging of aMECA-79-QDc with MECA-79 antibody blocking. Balb/c mice (n = 3) were first intravenously injected with free MECA-79 antibody (250 μg per mouse; blocking time: 24 hours), followed by a second intravenous injection of aMECA-79-QDc with the same does as the no blocking experiments. Wide-field imaging was performed 2 h and 24 h post injection of aMECA-79-QDc. (**e**) Wide-field imaging of Balb/c mice (n = 3) 10 min and 24 h post injection of TRC105-QDc. TRC105 is an irrelevant antibody to PNAd but is an antibody to endoglin overexpressed on proliferating endothelial cells. In (**a**,**d**,**e**) we did not observe apparent fluorescence signal in the inguinal lymph node. In contrast, in (**b**) the inguinal lymph node showed

strong signal 24 h post injection of aMECA-79-QDc intravenously, suggesting targeted iLN HEVs labeling by QDc conjugated with anti-MECA-79.

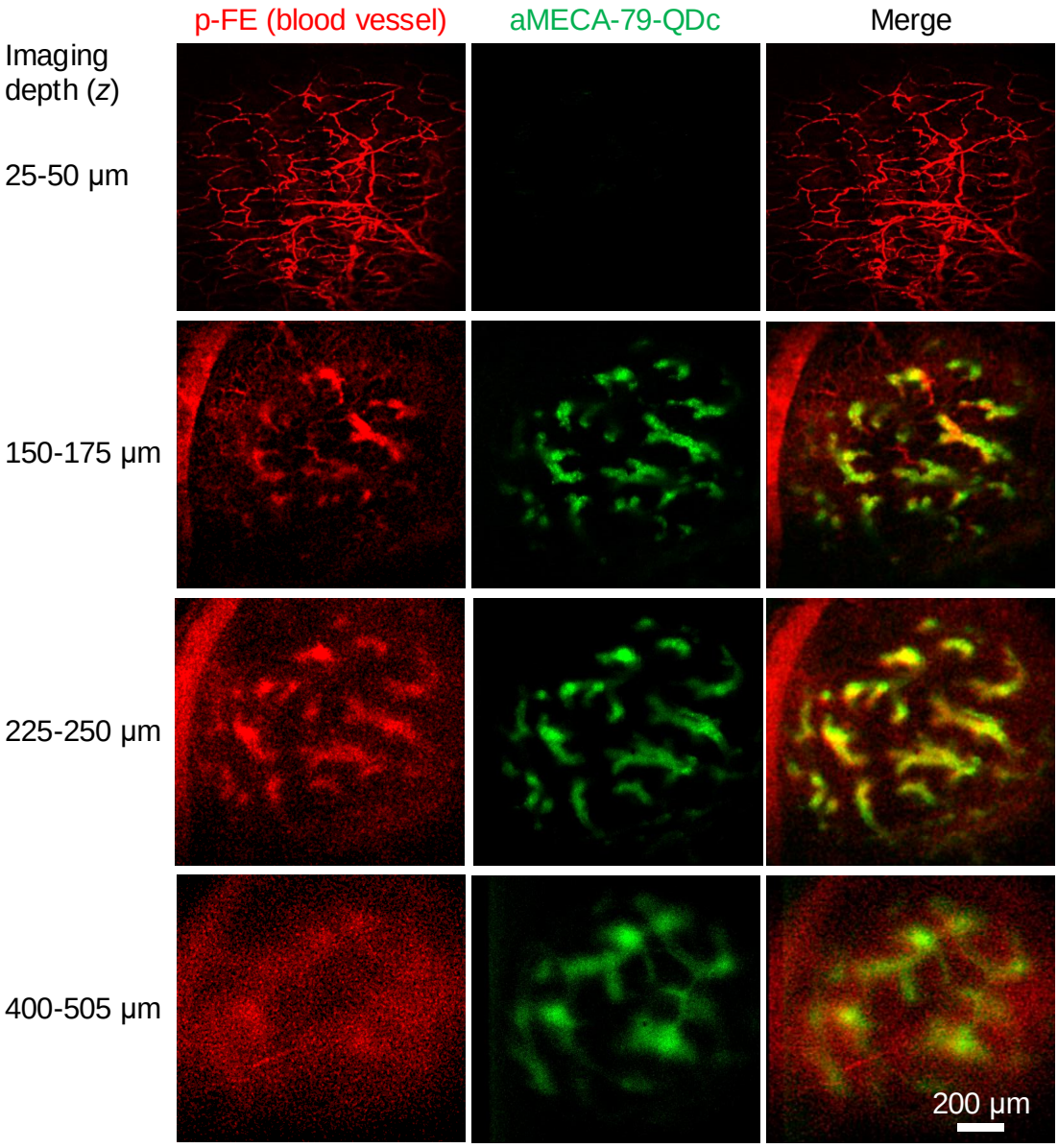

Supplementary Figure 9. Non-invasive two-color *in vivo* NIR-II confocal microscopy imaging of inguinal lymph nodes in mice at various depths under the skin. High-resolution confocal microscopy of blood vessels (red color, vessels contained circulating p-FE dye; excitation: 808 nm, emission: 1200-1400 nm) and HEVs in iLN targeted and labelled specifically by aMECA-79-QDc (green, excitation: 1540 nm, emission: 1750-2000 nm). Imaging was done with a 5 µm scan increment along *z* direction. The imaging time per plane was linearly increased from 5 s to 15 s from the first frame at the skin surface to the last plane inside the iLN. Imaging depths are labeled at the left of the figure. Notice that all vessels contained the circulating p-FE dye, and only HEVs were specifically targeted and labeled by the antibody-QDc conjugate. Similar results for n = 11 individuals (BALB/c, female, 3 weeks old).

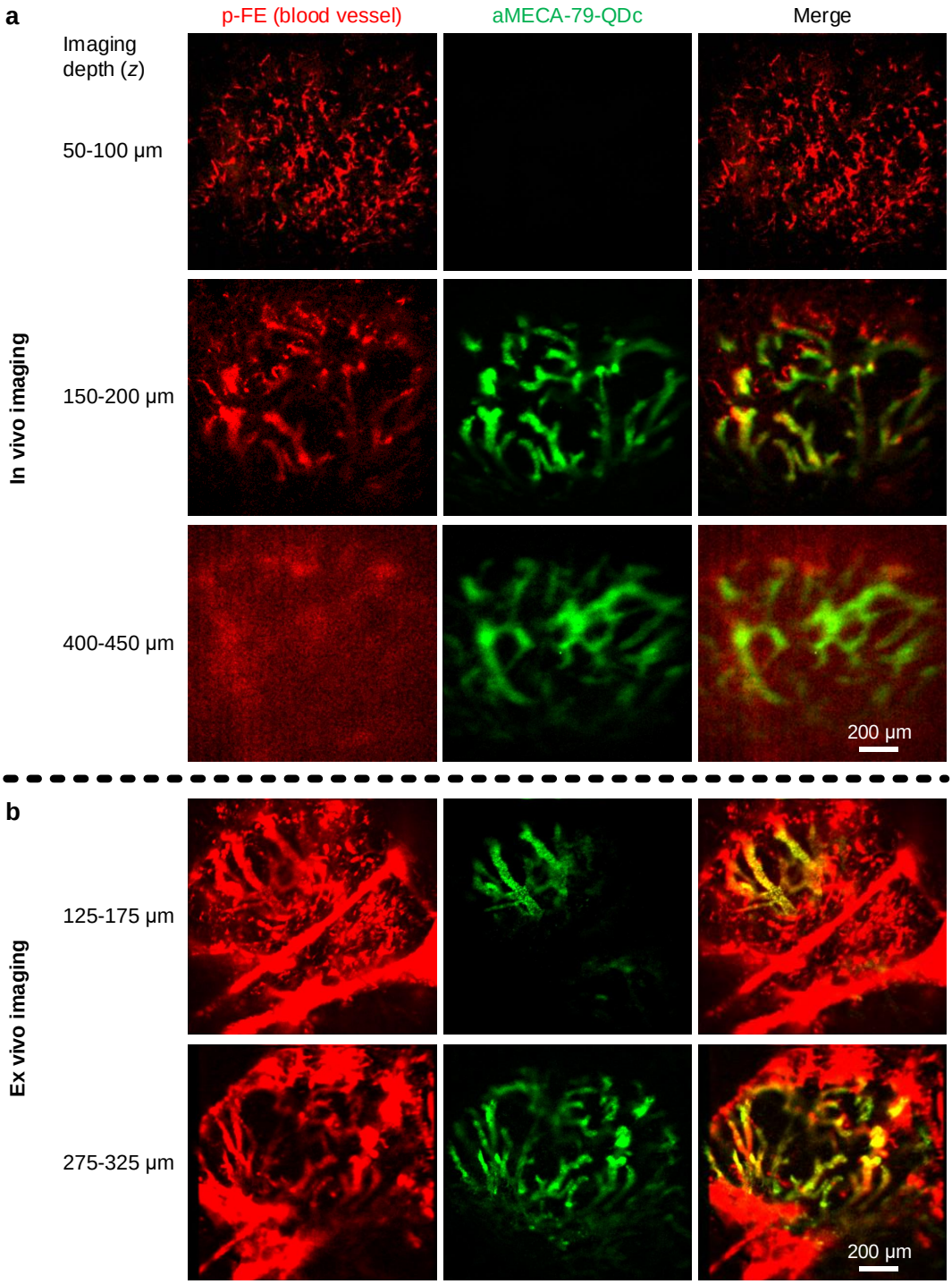

Supplementary Figure 10. NIR-IIc confocal microscopy imaging of inguinal lymph nodes in mice at various depths under the skin by using 1650 nm excitation. (**a**) Non-invasive confocal microscopy of blood vessels (red color, vessels contained circulating p-FE dye; excitation: 808 nm, emission: 1200-1400 nm) and HEVs labelled specifically by aMECA-79-QDc (green, excitation: 1650 nm, emission: 1800-2000 nm) in iLN. Imaging was done with a 10 μm scan increment along *z* direction. For NIR-IIc imaging, the imaging time per plane and the power of 1650 nm laser were linearly increased from 5 s to 15 s and from 1.6 mW to 10.0 mW, respectively, from the first frame at the skin surface to the last plane inside the iLN. (**b**) Ex vivo confocal microscopy of blood vessels and HEV vessels under the same imaging condition as (**a**). After experiments shown in (**a**), the mouse was euthanized under anesthesia. The iLN was taken out, fixed with 10% neutral-buffered

formalin at room temperature and preserved in glycerol at 4 ^{o}C for ex vivo imaging. The ex vivo results were similar to in vivo results that all vessels labelled by p-FE dye, and only HEVs were specifically labeled by the aMECA-79-QDc conjugate. Similar results for n = 11 individuals (BALB/c, female, 3 weeks old).

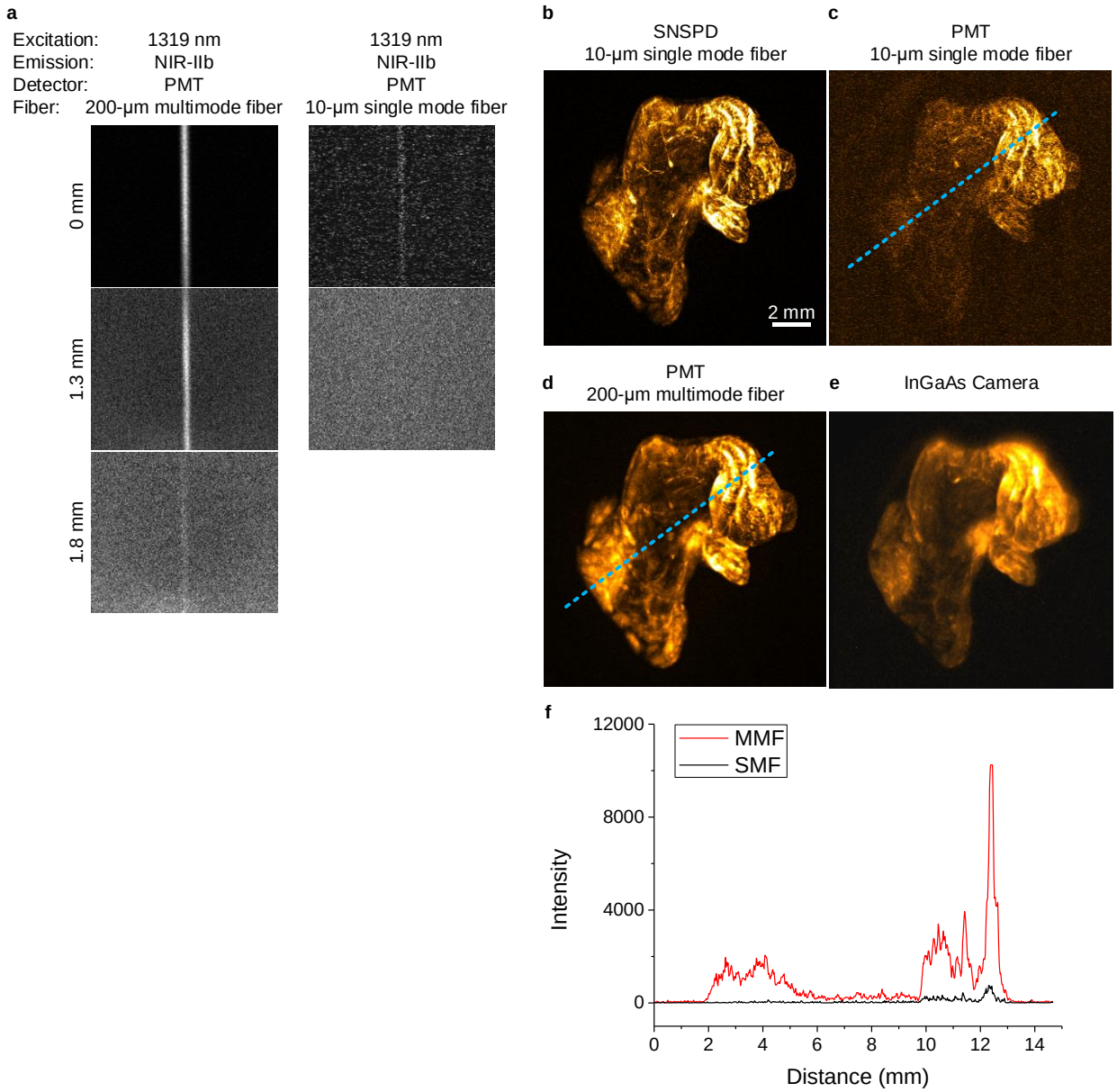

Supplementary Figure 11. (**a**) NIR-IIb confocal microscopy of a 50 µm capillary filled with QDb in 5% intralipid using 1319 nm excitation and an InGaAs PMT coupled with a 200-µm multimode fiber (M122L01, Thorlabs) or a 10.4-µm multimode fiber (P1-SMF28E-FC-5, Tholrabs). A 10X objective (NA = 0.25) was used. NIR-IIb fluorescence was collected in 1500-1700 nm. Similar results for n = 3 individual experiments. Ex vivo NIR-IIb confocal microscopy of blood vessels in mouse stomach using (**b**) SNSPD coupled with a 10.4-µm multimode fiber (P1-SMF28E-FC-5, Tholrabs), (**c**) PMT coupled with a 10.4-µm multimode fiber (P1-SMF28E-FC-5, Tholrabs) or (**d**) PMT coupled with a 200-µm multimode fiber (M122L01, Thorlabs) and (**e**) an InGaAs camera. The mouse was euthanized under anesthesia 20 min post intravenous injection of P^3-QDc while still in circulation. The mouse stomach was fixed with 10% neutral-buffered formalin at room temperature and preserved in glycerol at 4 ^{o}C for ex vivo imaging. An 808-nm laser was used for excitation. (**f**) Intensity profiles along the dotted lines in **c** and **d**.

a

Objectives	100X	25X	20X	20X	10X	5X
NA	0.8	1.05	0.75	0.4	0.25	0.12

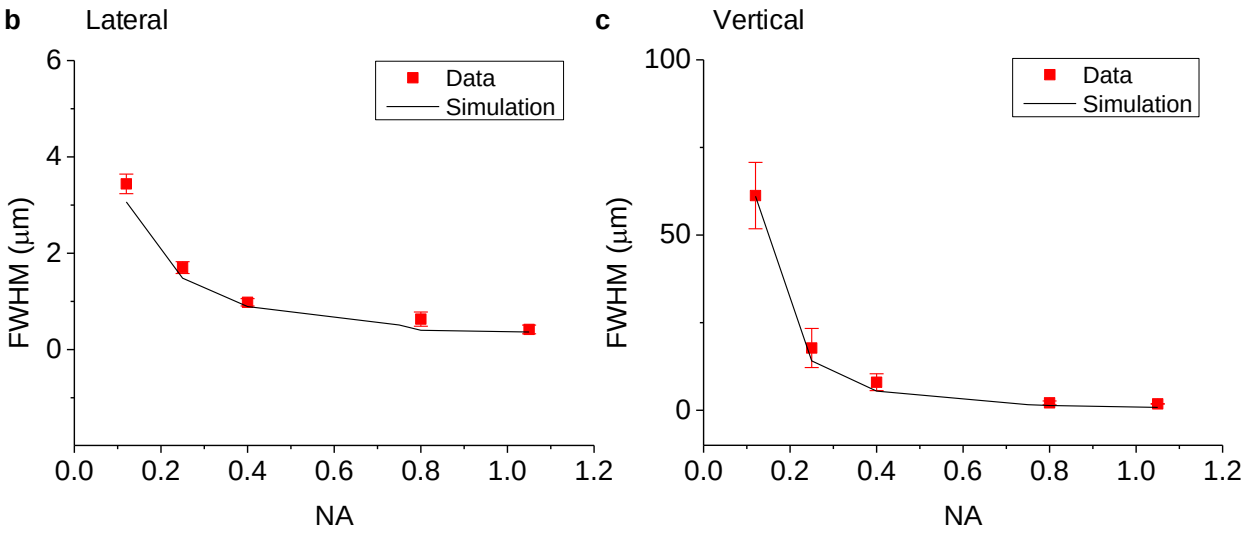

Supplementary Figure 12. Resolution of confocal microscopy with SNSPD analyzed by experimental measurements and theoretical calculations. (**a**) Objectives with different magnifications and numerical apertures were used in this analysis. Comparison of experimentally measured FWHMs and FWHMs of theoretically calculated PSFs in (**b**) lateral or (**c**) vertical directions. For experimental measurements, we imaged 300 nm polystyrene beads containing a NIR-II organic dye (p-FE)[6] (emission mostly in 1000-1300 nm range) with different objectives listed in (**a**) by the confocal microscope with SNSPD coupled to a single mode fiber with ~ 10-μm mode field diameter. Fluorescence emission > 1100 nm was collected and 658-nm laser was used. The FWHMs of nanoparticles in the lateral and vertical directions were measured from the confocal microscopy images. For calculation, the model in Supplementary Note 2 was used to calculate the PSF based on parameters the same as the experimental conditions. The FWHMs of PSFs were measured to compare with experimental measured FWHMs of beads with excellent agreement. (**b**,**c**) Data are shown as mean ± s.d. derived from analyzing > 5 independent polystyrene beads.

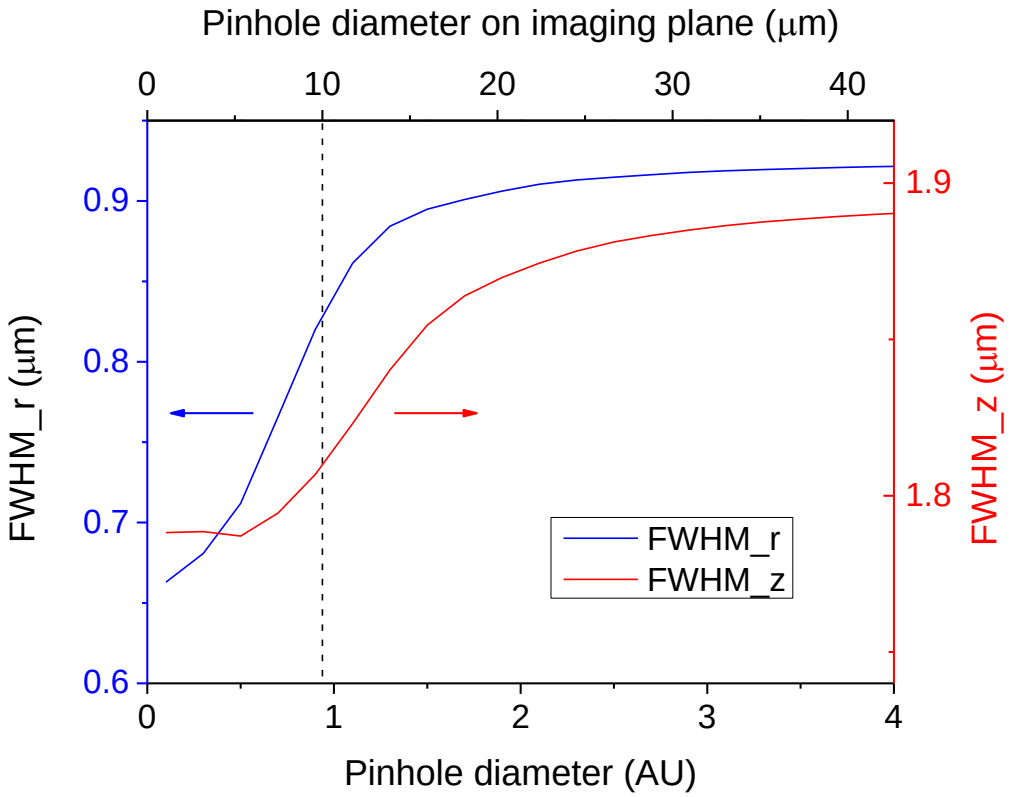

Supplementary Figure 13. The influence of the pinhole diameter on the resolution of NIR-IIc confocal microscopy. In this simulation, the excitation was 1650 nm and fluorescence emission was ~ 1850 nm. A 25X objective (NA = 1.05) was used. The pinhole diameter was normalized as Airy units, 1 AU = $1.21\lambda_d/NA_d$, where NA_d is the numerical aperture of objective. λ_d is the emission wavelength. A single mode fiber with ~ 10-μm mode field diameter (corresponding to ~ 0.94 AU, dash line) was used in our experiments and worked as a pinhole. This combination enables PSF with FWHMs of ~ 0.83 μm and ~ 1.82 μm in lateral and vertical direction, respectively

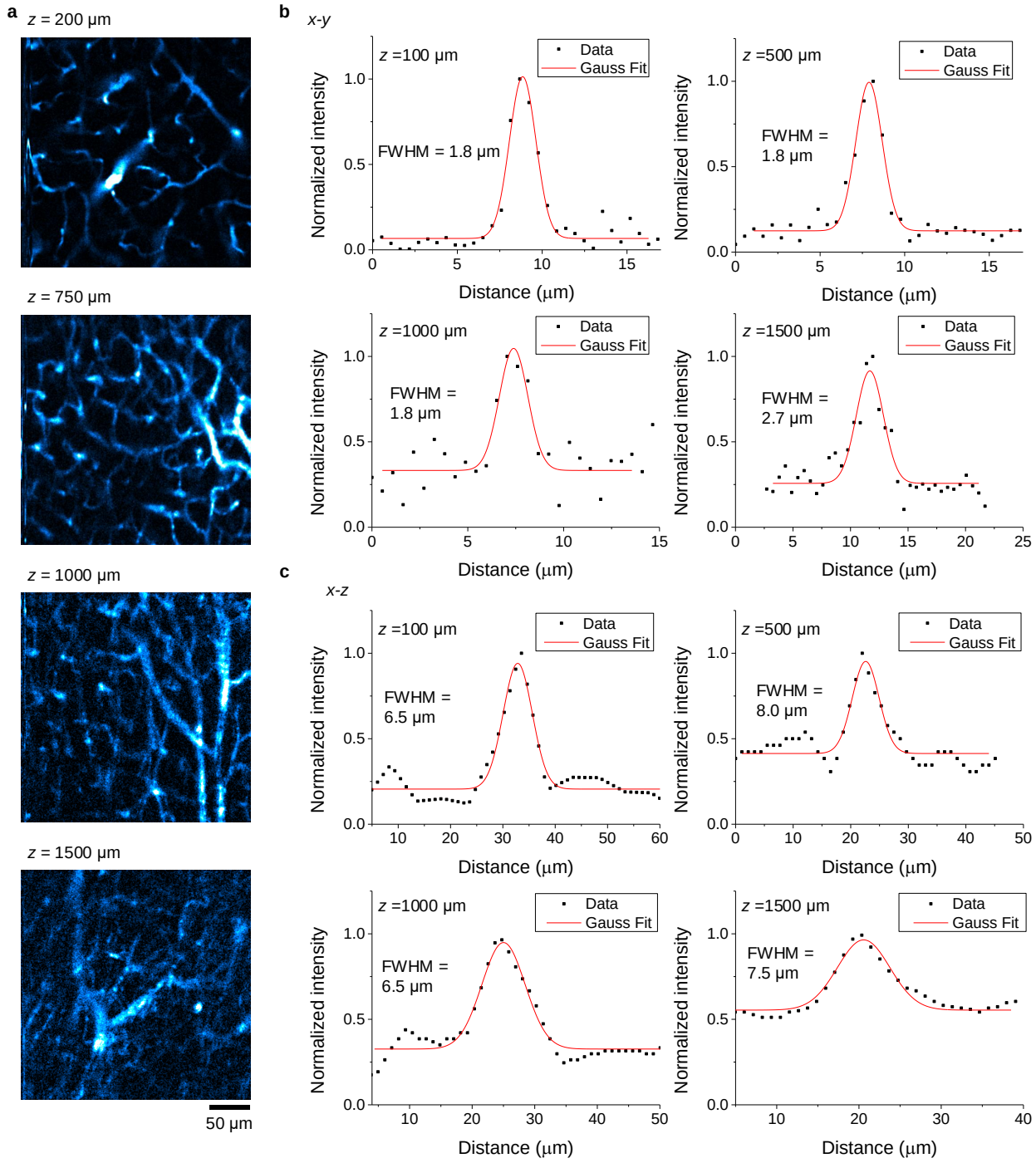

Supplementary Figure 14. Resolution estimation of NIR-IIc confocal microscopy with 1650 nm excitation by imaging blood vessels in mouse brain ex vivo. (**a**) Selected imaging layers at different imaging depth. FWHMs of blood vessels in (**b**) x-y plane or (**c**) x-z plane. These FWHMs set an upper limit of the resolution for NIR-IIc confocal microscopy. [7] The mouse brain tissue sample for ex vivo confocal microscopy was prepared by intravenous injection of free P^3-QDc. The mouse was euthanized under anesthesia 20 min post injection of P^3-QDc while still in circulation. The mouse brain (n = 2) was fixed with 10% neutral-buffered formalin at room temperature and preserved in glycerol at 4 ^oC for ex vivo imaging. A 1650 nm laser was used for excitation and a 25X (NA = 1.05) objective was used. The laser power at sample surface was 28.5 mW. The imaging

time per plane was linearly increased from 5 s to 20 s from the first frame at the scalp surface to the last plane inside the brain tissue. A 5-μm *z*-scan increment was applied for 3D imaging.

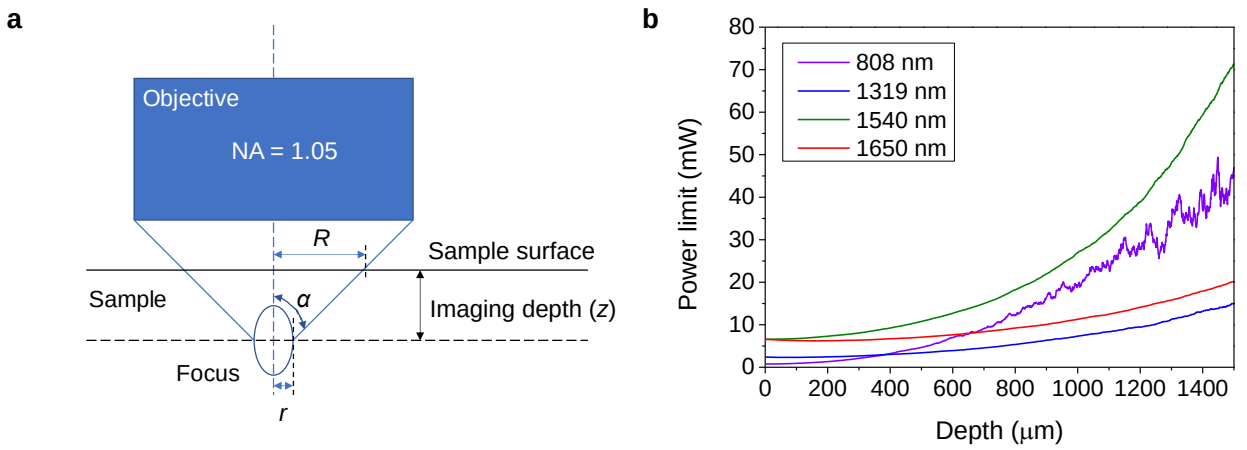

Supplementary Figure 15. (**a**) The relationship between the radius (*R*) of laser pattern on sample surface and imaging depth (*z*). (**b**) Power limit at mouse brain surface when imaging different depth. From the American National Standard for Safe Use of Lasers (ANSI Z136.1), the safety limit for 808 nm, 1319 nm, 1540 nm and 1650 nm lasers are 1.8 $t^{0.25}$ J cm^{-2}, 5.5 $t^{0.25}$ J cm^{-2}, 1.0 J cm^{-2} and 1.0 J cm^{-2}, which corresponds to 1.8 $A\,t^{-0.75}$ W, 5.5 $A\,t^{-0.75}$ W, $A\,t^{-1}$ W and $A\,t^{-1}$ W, respectively. Where *A* is spot area and can be derived from the point spread function[3] (see Supplementary Fig. 14). *t* is the dwell time. Dwell time was adjusted linearly from 19 μs to 57 μs from mouse brain surface (z = 0 mm) to z = 1.5 mm depth in brain. Consider the attenuation of laser transmitting in mouse brain (Supplementary Fig. 6c), we can get the threshold power at brain surface for confocal imaging at each depth.

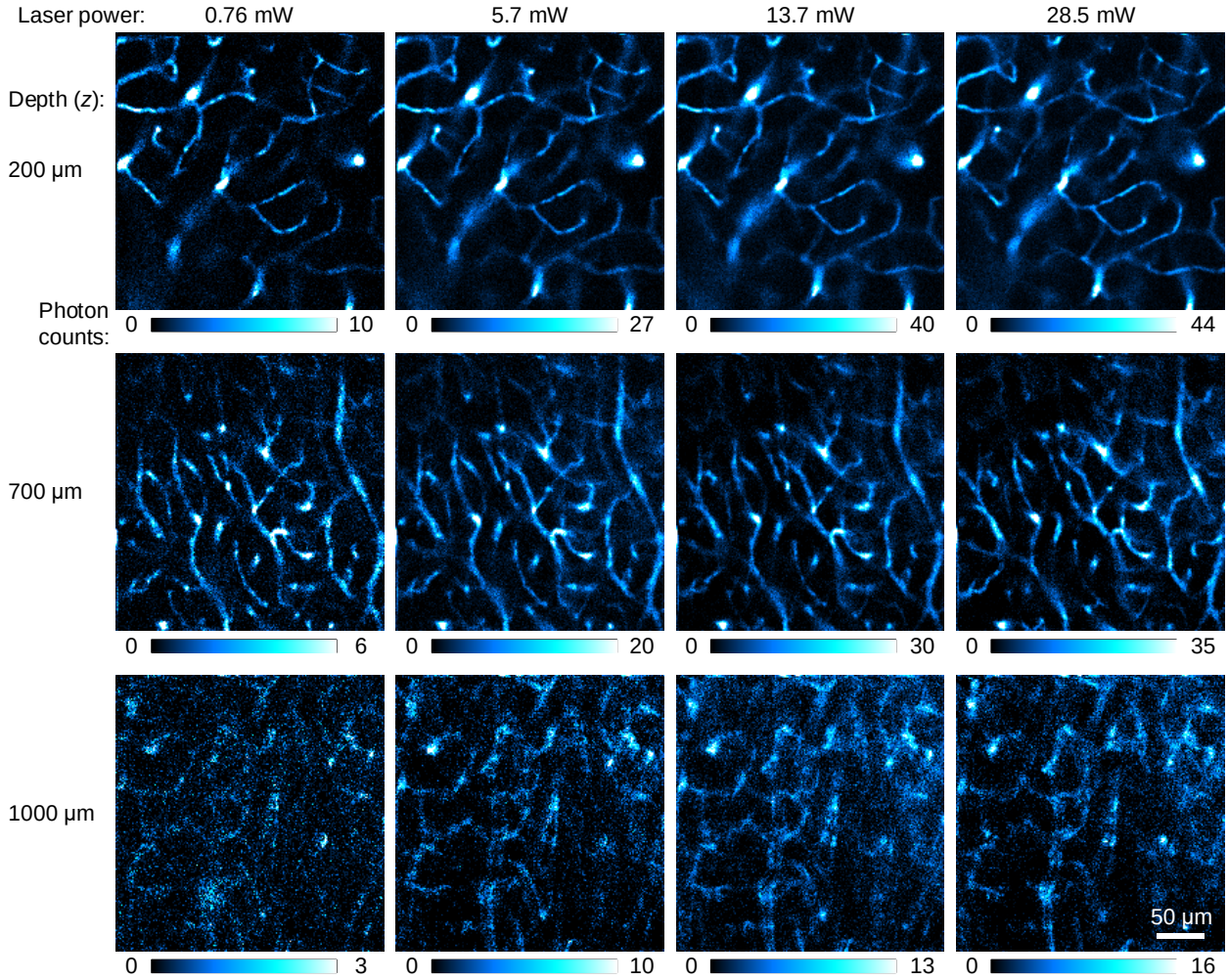

Supplementary Figure 16. The influence of 1650 nm laser's power on NIR-IIc confocal microscopy of blood vessels in mouse brain ex vivo. The mouse brain tissue sample (n = 2) for ex vivo confocal microscopy was prepared by intravenous injection of free P^3-QDc. The mouse was euthanized under anesthesia 20 min post injection of P^3-QDc while still in circulation. The mouse brain was fixed with 10% neutral-buffered formalin at room temperature and preserved in glycerol at 4 ^oC for ex vivo imaging. The power of 1650 nm laser at brain surface was modulated from 0.76 mW to 28.5 mW. A fixed scan time per frame of 2 s for all position was used. The pixels per frame were 200 x 200. An 100 µm scan step in *z* and a 25 X objective (NA = 1.05) was used.

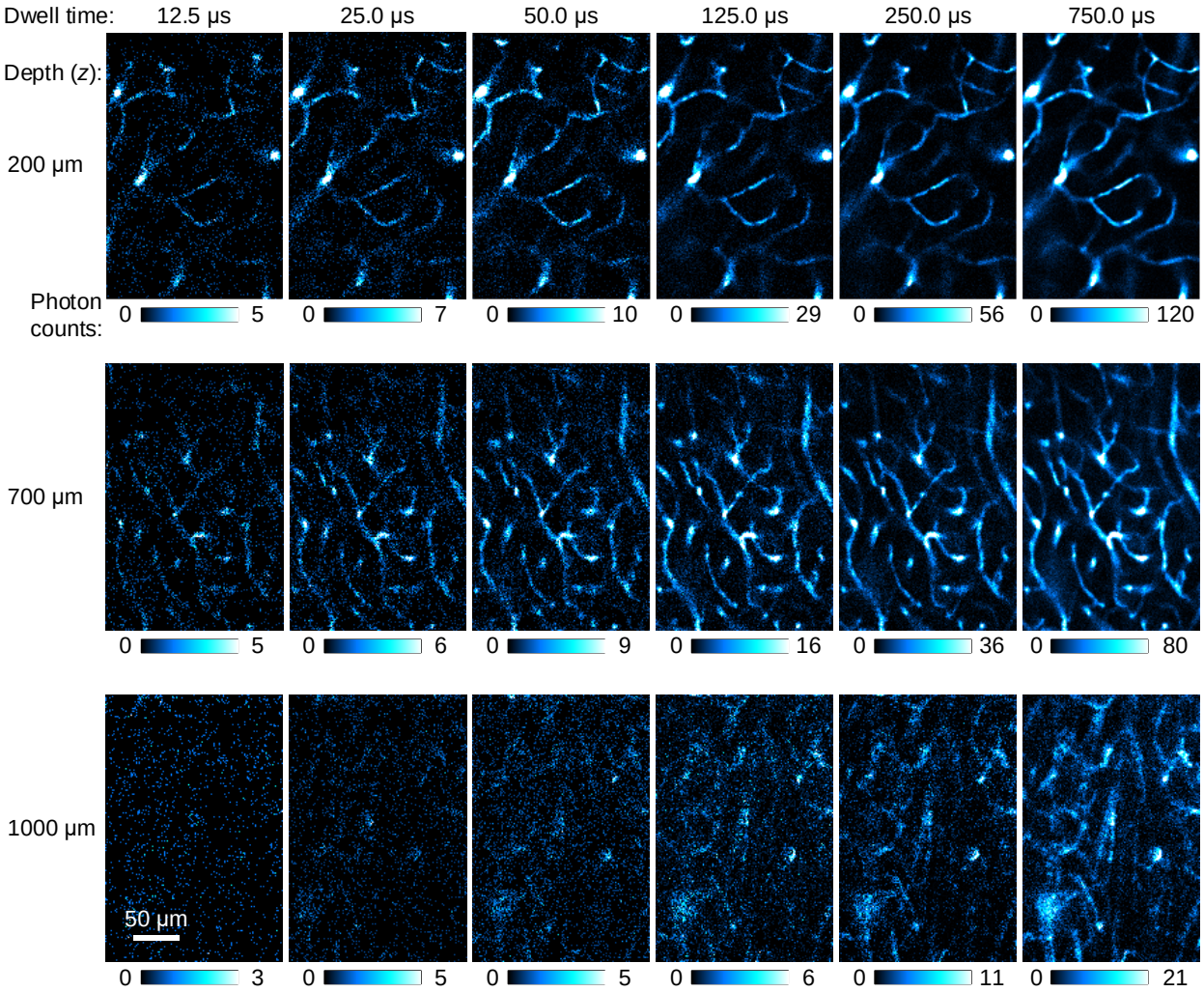

Supplementary Figure 17. The influence of dwell time on NIR-IIc confocal microscopy of blood vessels in mouse brain under 1650 nm excitation ex vivo. The same mouse brain tissue (n = 2) as the one used in Supplementary Fig. 16. A fixed laser power of 0.76 mW at brain surface was used for all imaging. The dwell time increased from 12.5 µs to 750.0 µs. An 100 µm scan step in *z* and a 25 X objective (NA = 1.05) was used.

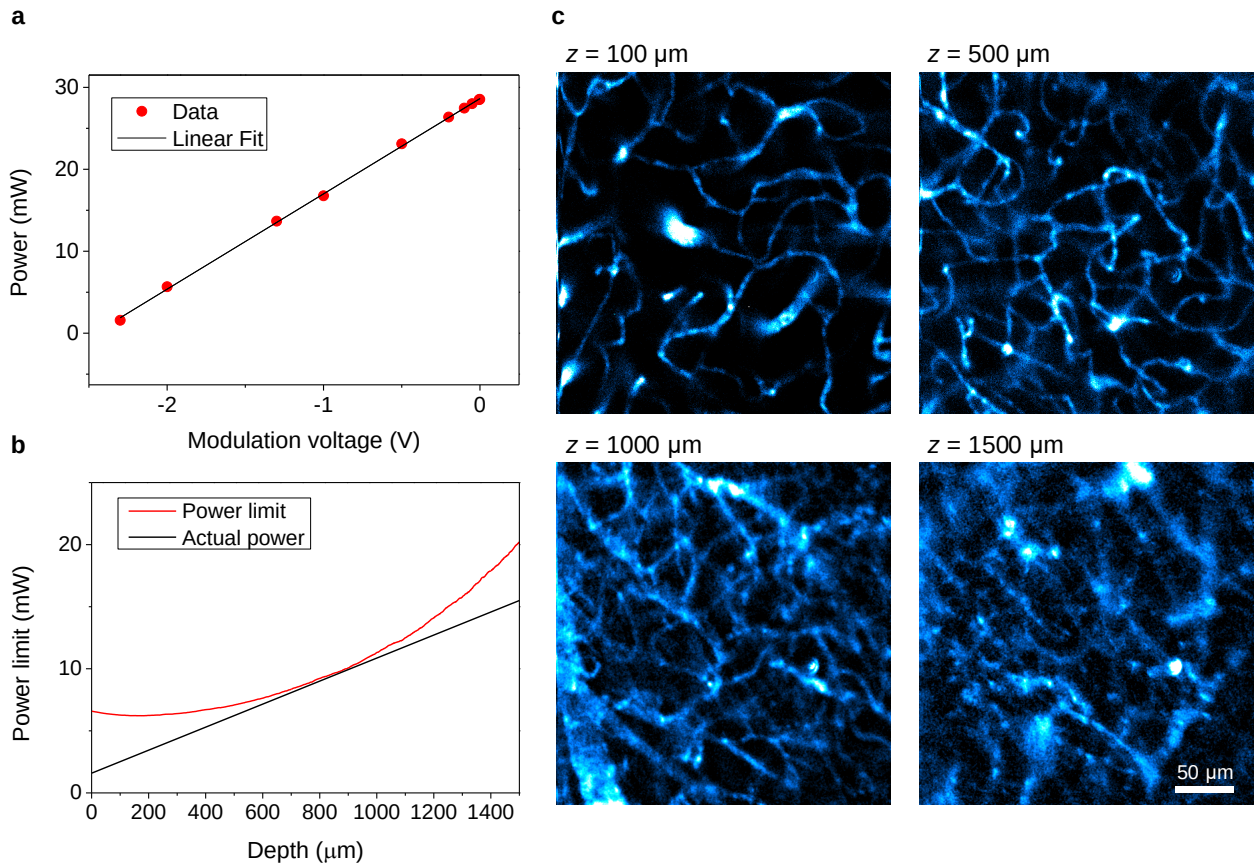

Supplementary Figure 18. NIR-IIc confocal microscopy of blood vessels in mouse brain ex vivo by using a 1650 nm laser with power modulated linearly. (**a**) The relationship between laser power at brain surface and external modulation voltage. (**b**) The laser power at brain surface was linearly adjusted from 1.6 mW to 15.5 mW from the first frame at the brain surface to the last plane inside the brain tissue (n = 2). The laser power used here was below the power limit at every imaging depth. Complex external modulation voltage can also be applied to follow the tendency of the power limit and prevent laser damage. (**c**) NIR-IIc confocal microscopy of blood vessels in mouse brain at different imaging depth by using the laser power shown in **b**. The same mouse brain tissue as the one used in Supplementary Fig. 16. The imaging time per plane was linearly increased from 5 s to 15 s from the first frame at the brain surface to the last plane inside the brain tissue. A 10 μm scan step in *z* and a 25 X objective (NA = 1.05) was used. The pixels per frame were 512 x 512.

Supplementary Table 1. Imaging conditions

	Contrast agent	Excitation (nm) (Power/ intensity)	Emission (nm)	Scan time per plane (s) (total imaging time for 3D imaging)	Pixels in *xy* (pixel size)	Scan step in *z* (μm)	Objective (NA)
Fig. 3b left	P^3-QDc	1540 (35 mW)	1750-2000	5-30 (47.3 min)	512x512 (1.1 μm)	5	25X (1.05)
Fig. 3b right	P^3-QDc	1650 (28.5 mW)	1800-2000	5-20 (47.3 min)	512x512 (1.1 μm)	5	25X (1.05)
Fig. 3c first column	P^3-QDb	1319 (28.5 mW)	1500-1700	5-20 (11.8 min)	512x512 (1.1 μm)	20	25X (1.05)
Fig. 3c second column	P^3-QDb	1319 (28.5 mW)	1500-1700	5-20 (11.8 min)	512x512 (1.1 μm)	20	25X (1.05)
Fig. 3c third column	P^3-QDc	1540 (28.5 mW)	1800-2000	5-20 (11.8 min)	512x512 (1.1 μm)	20	25X (1.05)
Fig. 3c forth column	P^3-QDc	1650 (28.5 mW)	1800-2000	5-20 (47.3 min)	512x512 (1.1 μm)	5	25X (1.05)
Fig.4b	p-FE	808 (70 mW cm^{-2})	1200-1400	0.03 (/)	640x512 (/)	/	Wide-field, whole body
	aMECA-79-QDc	808 (70 mW cm^{-2})	1500-1700	0.04 (/)	640x512 (/)	/	Wide-field, whole body
Fig.4c left	p-FE	808 (70 mW cm^{-2})	1200-1400	0.04 (/)	640x512 (/)	/	Wide-field, 5X
	aMECA-79-QDc	808 (70 mW cm^{-2})	1500-1700	0.04 (/)	640x512 (/)	/	Wide-field ,5X
Fig.4c right	p-FE	808 (3.5 mW)	1200-1400	25.0 (/)	512x512 (12.1 μm)	/	5X
	aMECA-79-QDc	1540 (28.5 mW)	1750-2000	25.0 (/)	512x512 (12.1 μm)	/	5X
Fig.4d	p-FE	808 (3.5 mW)	1200-1400	5-15.0 (16.7 min)	512x512 (2.7 μm)	5	25X

	aMECA-79-QDc	1540 (35 mW)	1750-2000	5-15 (16.7 min)	512x512 (2.7 μm)	5	25X
Fig.4e	aMECA-79-QDc	1540 (35 mW)	1750-2000	10 (/)	512x512 (2.7 μm)	/	25X
Fig. 4f	aCD169-QDa	808 (70 mW cm^{-2})	1200-1400	0.01 (/)	640x512 (/)	/	Wide-field, whole body
	aCD3-QDc	808 (70 mW cm^{-2})	1500-1700	0.05 (/)	640x512 (/)	/	Wide-field, whole body
Fig. 4g,h	aCD169-QDa	808 (3.5 mW)	1200-1400	8-30 (20.6 min)	512x512 (2.4 μm)	10	25X
	aCD3-QDc	1650 (1.6-10.0 mW)	1800-2000	5-12 (10.0 min)	512x512 (2.4 μm)	10	25X
Fig. 4i	aCD3-QDc	1650 (1.6-10.0 mW)	1800-2000	60 (10.0 min)	512x512 (0.27 μm)	50	25X
Fig. 4j	DRAQ7	658 (1.5 mW)	790-850	60 (/)	512x512 (0.27 μm)	/	25X
	aCD3-QDc	1650 (28.5 mW)	1800-2000	60 (/)	512x512 (0.27 μm)	/	25X
Supplementary Fig. 7	P^3-QDc	1650 (0.76-28.5 mW)	1800-2000	0.34 (1.1 min)	133x200 (1.39 μm)	5	25X
Supplementary Fig. 8a	P^3-QDc	808 (70 mW cm^{-2})	1500-1700	0.05	640x512 (/)	/	Wide-field, whole body
Supplementary Fig. 8b	aMECA-79-QDc	808 (70 mW cm^{-2})	1500-1700	0.05	640x512 (/)	/	Wide-field, whole body
Supplementary Fig. 8d	aMECA-79-QDc	808 (70 mW cm^{-2})	1500-1700	0.05	640x512 (/)	/	Wide-field, whole body
Supplementary Fig. 8e	TRC105-QDc	808 (70 mW cm^{-2})	1500-1700	0.05	640x512 (/)	/	Wide-field, whole body
	p-FE	808	1200-1400	5-15	512x512	5	25X

Supplementary Fig. 9		(3.5 mW)		(16.7 min)	(2.7 μm)		
	aMECA-79-QDc	1540 (28.5 mW)	1750-2000	5-15 (16.7 min)	512x512 (2.7 μm)	5	25X
Supplementary Fig. 10	p-FE	808 (3.5 mW)	1200-1400	8-30 (20.6 min)	512x512 (2.4 μm)	10	25X
	aMECA-79-QDc	1650 (1.6-10.0 mW)	1800-2000	5-15 (10.8 min)	512x512 (2.4 μm)	10	25X
Supplementary Fig. 14	P^3-QDc	1650 (28.5 mW)	1800-2000	5-20 (62.5 min)	512x512 (0.54 μm)	5	25X
Supplementary Fig. 16	P^3-QDc	1650 (0.76-28.5 mW)	1800-2000	2 (20.0 s)	200x200 (1.39 μm)	100	25X
Supplementary Fig. 17	P^3-QDc	1650 (0.76 mW)	1800-2000	0.34-20 (/)	133x200 (1.39 μm)	100	25X
Supplementary Fig. 18	P^3-QDc	1650 (1.6-15.5 mW)	1800-2000	5-15 (25.0 min)	512x512 (0.54 μm)	10	25X

Supplementary Table 2. Comparison between NIR-IIc confocal and three-photon microscopy at ~1700-nm excitation.

<table>
<tr><th></th><th>Three-photon microscopy[7,8]</th><th>NIR-IIc confocal microscopy</th></tr>
<tr><td>Excitation Wavelength</td><td>1680 nm</td><td>1650 nm</td></tr>
<tr><td>Emission wavelength</td><td>~ 630 nm</td><td>1800-2000 nm</td></tr>
<tr><td>Laser
(laser cost)</td><td>Femtosecond laser
(~320k USD)</td><td>CW laser
(~4k USD)</td></tr>
<tr><td>Laser power</td><td>3 – 35 mW</td><td>0.6 – 28.5 mW</td></tr>
<tr><td rowspan="2">Resolution</td><td rowspan="2">XY: 0.9 µm
Z: 5.4 µm</td><td>Theoretical resolution:
XY: 0.84 µm
Z: 1.86 µm</td></tr>
<tr><td>Resolution estimated by imaging blood vessels in mouse brain ex vivo:
XY: 2.0 ± 0.45 µm
Z: 7.1 ± 0.75 µm</td></tr>
<tr><td>Objective</td><td colspan="2">Olympus XLPLN25XWMP2; 25× /1.05-NA</td></tr>
<tr><td>Frame time
(Area)
(Pixels per frame)</td><td>8 – 20 s
(122 µm × 122 µm)
(512 × 512)</td><td>5 – 20 s
(550 µm × 550 µm)
(512 × 512)</td></tr>
<tr><td rowspan="2">Imaging depth</td><td>1400 µm
(1680 nm excitation, scalp and skull removed, 10-week-old FVB/N mice)[7]</td><td rowspan="2">1135 µm
(through intact skin and skull, 3-week-old BALB/c mice)</td></tr>
<tr><td>700 µm
(1319 nm, through intact skull with scalp removed, 12-week-old B6.Cg-Tg(Thy1-Brainbow1.0)HLich/J mice)[9]</td></tr>
<tr><td rowspan="2">Signal-to-background ratio
(SBR)</td><td>~ 100
(1680 nm excitation, three-photon microscopy, scalp and skull removed, 10-week-old FVB/N mice)[7]</td><td rowspan="2">5 – 169
(through intact skin and skull, 3-week-old BALB/c mice)</td></tr>
<tr><td>Two-photon microscopy: 2.0 – 4.0
Three-photon microscopy: 8.5 – 80.0
(1319 nm excitation, through intact skull with scalp removed, C57BL/6J, male, 12 weeks old)[9]</td></tr>
</table>

Supplementary Table 3. Average laser power used in two-photon or three-photon microscopy.

Excitation wavelength (nm)	Average laser power (mW)	Reference
775	52-60	10
920	18-250	11-13
970	36-120	14
1280	11.5-100	10
1320	50 – 110	9,11,15,16
1450	35	8
1500	35	8
1550	35	8
1617	56	17
1680	3 – 35	7
1700	1.4 – 100	12,15,18

Supplementary References:

1. Chang, J. *et al.* Multimode-fiber-coupled superconducting nanowire single-photon detectors with high detection efficiency and time resolution. *Appl. Opt.* **58**, 9803-9807 (2019).
2. Liao, J. *et al.* Depth-resolved NIR-II fluorescence mesoscope. *Biomed. Opt. Express* **11**, 2366-2372 (2020).
3. Yildirim, M., Sugihara, H., So, P. T. C. & Sur, M. Functional imaging of visual cortical layers and subplate in awake mice with optimized three-photon microscopy. *Nature Communications* **10**, 177 (2019).
4. Mertz, J. *Introduction to optical microscopy*. (Cambridge University Press, 2019).
5. Wang, L., Jacques, S. L. & Zheng, L. MCML—Monte Carlo modeling of light transport in multi-layered tissues. *Comput. Meth. Prog. Bio.* **47**, 131-146 (1995).
6. Wan, H. *et al.* A bright organic NIR-II nanofluorophore for three-dimensional imaging into biological tissues. *Nature communications* **9**, 1-9 (2018).
7. Horton, N. G. *et al.* In vivo three-photon microscopy of subcortical structures within an intact mouse brain. *Nature Photonics* **7**, 205-209 (2013).
8. Wang, M. *et al.* Comparing the effective attenuation lengths for long wavelength in vivo imaging of the mouse brain. *Biomed. Opt. Express* **9**, 3534-3543 (2018).
9. Wang, T. *et al.* Three-photon imaging of mouse brain structure and function through the intact skull. *Nature Methods* **15**, 789-792 (2018).
10. Kobat, D. *et al.* Deep tissue multiphoton microscopy using longer wavelength excitation. *Opt. Express* **17**, 13354-13364 (2009).
11. Ouzounov, D. G. *et al.* In vivo three-photon imaging of activity of GCaMP6-labeled neurons deep in intact mouse brain. *Nature Methods* **14**, 388-390 (2017).
12. Li, B., Wu, C., Wang, M., Charan, K. & Xu, C. An adaptive excitation source for high-speed multiphoton microscopy. *Nature Methods* **17**, 163-166 (2020).
13. Podgorski, K. & Ranganathan, G. Brain heating induced by near-infrared lasers during multiphoton microscopy. *Journal of Neurophysiology* **116**, 1012-1023 (2016).
14. Lu, R. *et al.* Rapid mesoscale volumetric imaging of neural activity with synaptic resolution. *Nature Methods* **17**, 291-294 (2020).
15. Guesmi, K. *et al.* Dual-color deep-tissue three-photon microscopy with a multiband infrared laser. *Light: Science & Applications* **7**, 12 (2018).
16. Hontani, Y., Xia, F. & Xu, C. Multicolor three-photon fluorescence imaging with single-wavelength excitation deep in mouse brain. *Science Advances* **7**, eabf3531 (2021).
17. Cheng, H. *et al.* Deep-brain 2-photon fluorescence microscopy in vivo excited at the1700 nm window. *Opt. Lett.* **44**, 4432-4435 (2019).
18. Horton, N. G. & Xu, C. Dispersion compensation in three-photon fluorescence microscopy at 1,700 nm. *Biomed. Opt. Express* **6**, 1392-1397 (2015).